

Compressed Coding, AMP Based Decoding and Analog Spatial Coupling

Shansuo Liang, Chulong Liang, Junjie Ma, and Li Ping, *Fellow, IEEE*

Abstract

This paper considers a compressed coding (CC) scheme that combines compressed sensing with forward error control coding. Approximate message passing (AMP) is used to decode the message. Based on the state evolution analysis of AMP, we derive the performance limit of the CC scheme. We show that the CC scheme can approach Gaussian capacity at a very high compression ratio. Further, the results are extended to systems involving non-linear effects such as clipping. We show that the capacity approaching property can still be maintained when generalized AMP is used to decode the message.

To approach the capacity, a low-rate underlying code should be designed according to the curve matching principle, which is complicated in practice. Instead, analog spatial coupling (ASC) is used to avoid sophisticated low-rate code design. In the end, we study ASC-CC in a multiuser environment, where ASC can be realized in a distributive way. The overall block length can be shared by many users, which reduces block length per-user.

Index Terms

Compressed sensing, forward error control coding, approximate message passing, state evolution, area theorem and spatial coupling.

S. Liang, C. Liang and L. Ping are with Department of Electrical Engineering, City University of Hong Kong, Hong Kong SAR, China (e-mail: sliang3-c@my.cityu.edu.hk, liangchulong@qq.com, eeliping@cityu.edu.hk). J. Ma is with the John A. Paulson School of Engineering and Applied Sciences, Harvard University, Cambridge, MA 02138, USA (e-mail: junjiema@seas.harvard.edu).

This paper was presented in part at the 2016 9th International Symposium on Turbo Codes and Iterative Information Processing [1].

I. INTRODUCTION

Approximate message passing (AMP) has recently attracted many research attentions [2], [3]. The AMP algorithm can potentially outperform the conventional turbo algorithm in systems involving sensing matrices with independent and identically distributed (i.i.d.) Gaussian entries [4]. The convergence behavior of AMP can be rigorously analyzed using a state evolution (SE) technique [3]. In particular, AMP has been applied to decode sparse-regression (SR) codes, which are constructed using position modulation followed by a compression matrix [5], [6].

Spatial coupling (SC) offers improved performance for turbo and LDPC type codes [7], [8]. Most works on SC are based on binary additions [7]–[10]. Analog SC schemes over real or complex fields have been investigated, such as the code division multiple access (CDMA) scheme in [11] and the data coupling (DC) scheme in [12]. It is shown that DC can approach Gaussian capacity at asymptotically high signal-to-noise-ratio (SNR). This is theoretically interesting but the SNR range is outside the scope of most practical systems.

SC has been applied to SR codes and the resultant SCSR code is asymptotically capacity approaching at high SNR [6], [13]. However, SCSR codes require a very high compression ratio to offer good performance at low to medium SNR ranges, where many practical communication systems are operating in. For this reason, most available simulation results of SCSR are for the high SNR scenario.

It is interesting to explore techniques that can improve the performance of SCSR codes at low to medium SNR. In a broader sense, it is interesting to study general impacts of introducing AMP into forward error control (FEC) decoding. Intuitively, AMP operates on a continuous field while FEC decoding on a discrete field. Also, AMP is originally studied for compressed sensing and FEC coding is studied for error control. What are the benefits of combining them?

This paper is motivated by the above questions. We study a compressed coding (CC) scheme, in which an FEC coded and modulated sequence is compressed by a sensing matrix before transmission [1], [14]. AMP is applied to decode the message. We investigate the related capacity limit, code construction methods and potential advantages. Our main findings are as follows.

- We derive the performance limit of the CC scheme under AMP based decoding. Our basic assumption

is that the SE for AMP remains accurate in the presence of an FEC decoder. Based on the area property of extrinsic information transfer (EXIT) charts, we show that CC can approach Gaussian capacity at a high compression ratio, even though the underlying coded sequence is non-Gaussian. This is consistent with the Gaussian distribution of the signals after compression.

- We extend the results to systems involving non-linear effects such as clipping and quantization. We show that the capacity approaching property can be maintained in such cases. This alleviates the problem of high peak to average power ratio (PAPR) related to Gaussian signaling.
- The above-mentioned capacity approaching properties require properly designed low-rate codes with matched EXIT curves, which can be difficult in practice [15]–[17]. We will introduce an analog spatial coupling (ASC) technique to avoid this difficulty.
- A code is said to be universal if it remains good after random puncturing. Such codes are useful in, e.g., type-II automatic repeat request (ARQ) applications [18]–[20]. The existing high-rate coded modulation methods typically do not work well after heavy puncturing. We show that the combined ASC and CC (ASC-CC) scheme is inherently universal. This provides a simple and efficient method for universal code design.
- We study ASC-CC in a multiuser environment. A traditional view is that ASC will increase overall block length, which causes difficulty in applications with stringent latency requirements. Interestingly, in a multi-user system, ASC-CC can be realized in a distributive way and the overall block length can be shared by many users, which effectively reduces block length per-user. Since many wireless systems are meant for multi-users by nature, the ASC-CC scheme is practically attractive.

In summary, the proposed ASC-CC scheme offers practical solutions to some well-known challenges in coding techniques: (i) a simple method to approach the ultimate capacity of Gaussian signaling (beyond that of discrete signaling), (ii) a simple treatment of non-linear effects during transmission, (iii) a low-cost universal coding and decoding strategy and (iv) a multi-user scheme with short per-user block length and good performance. These claims are supported by extensive theoretical and numerical results.

II. COMPRESSED CODING SCHEME

A. Transmitter Structure

Let $\mathbf{c} \in \mathbb{R}^{N \times 1}$ be a coded and modulated sequence based on an FEC code \mathcal{C} and a constellation $\mathcal{S} \equiv \{s_j\}$. We assume that the entries of \mathbf{c} are drawn from \mathcal{S} with equal probabilities and $\mathbb{E}[|s_j|^2] = 1$. The transmitted signal is given by $\mathbf{x} \triangleq \mathbf{A}\mathbf{c}$ as illustrated in Fig. 1(a). Assume an additive white Gaussian noise (AWGN) channel. The received signal $\mathbf{y} \in \mathbb{R}^{M \times 1}$ is given by ¹

$$\mathbf{y} = \mathbf{x} + \mathbf{n} = \mathbf{A}\mathbf{c} + \mathbf{n}, \quad (1)$$

where $\mathbf{n} \sim \mathcal{N}(\mathbf{0}, \sigma^2 \mathbf{I})$ contains AWGN samples. For theoretical analysis, we assume that the entries of $\mathbf{A} \in \mathbb{R}^{M \times N}$ are i.i.d. as $A_{m,n} \sim \mathcal{N}(0, 1/N)$. Denote R_C and R_{AC} the information rate of \mathbf{c} and $\mathbf{A}\mathbf{c}$, respectively. Defining $\delta \triangleq M/N$, we have $R_{AC} = R_C/\delta$. When R_C is fixed, R_{AC} can be adjusted by choosing different values of δ .

B. AMP Receiver

AMP is a low-complexity iterative algorithm for signal recovery from noisy measurements [2], [5], [6]. Initializing from $\mathbf{c}^1 = \mathbf{0}$ and $\mathbf{r}_{\text{Onsager}}^1 = \mathbf{0}$, the AMP algorithm alternates between a linear estimator (LE) and a nonlinear estimator (NLE) as [2], [5], [6]

$$\text{LE : } \quad \mathbf{r}^t = \hat{\mathbf{c}}^t + \mathbf{A}^T(\mathbf{y} - \mathbf{A}\hat{\mathbf{c}}^t) + \mathbf{r}_{\text{Onsager}}^t, \quad (2a)$$

$$\text{NLE : } \quad \hat{\mathbf{c}}^{t+1} = \eta(\mathbf{r}^t), \quad (2b)$$

where η is a denoising function of \mathbf{r}^t and $\mathbf{r}_{\text{Onsager}}^t$ in (2a) is an ‘‘Onsager’’ term defined as

$$\mathbf{r}_{\text{Onsager}}^t = \frac{N}{M} \cdot \left(\frac{1}{N} \sum_{n=1}^N \eta'(r_n^{t-1}) \right) (\mathbf{r}^{t-1} - \mathbf{c}^{t-1}). \quad (3)$$

¹In this paper, we focus on real-valued systems for the convenience of discussion. However, the related analyses and discussions can be extended to complex-valued systems by writing as the following real-valued model:

$$\begin{bmatrix} \text{Re}\{\mathbf{y}\} \\ \text{Im}\{\mathbf{y}\} \end{bmatrix} = \begin{bmatrix} \text{Re}\{\mathbf{A}\} & -\text{Im}\{\mathbf{A}\} \\ \text{Im}\{\mathbf{A}\} & \text{Re}\{\mathbf{A}\} \end{bmatrix} \begin{bmatrix} \text{Re}\{\mathbf{c}\} \\ \text{Im}\{\mathbf{c}\} \end{bmatrix} + \begin{bmatrix} \text{Re}\{\mathbf{n}\} \\ \text{Im}\{\mathbf{n}\} \end{bmatrix}.$$

The final estimate is given by $\hat{\mathbf{c}}^{T+1}$, where T is the maximum number of iterations. LE is used to handle the linear observation constraint $\mathbf{y} = \mathbf{A}\mathbf{c} + \mathbf{n}$ while NLE is used to explore the prior information of \mathbf{c} . The Onsager term is used to regulate correlation among messages during iterative processing. Fig. 1(b) illustrates the iterative process.

In this paper, the denoising function η in (2b) is given by an *a posteriori* probability (APP) decoder (DEC) for the underlying FEC code \mathcal{C} . Its input \mathbf{r}^t generated in (2a) is treated as a noisy observation of \mathbf{c} using the following model [5], [6]

$$\mathbf{r}^t = \mathbf{c} + (\rho^t)^{-1} \cdot \mathbf{w}, \quad (4)$$

where $\mathbf{w} \sim \mathcal{N}(\mathbf{0}, \mathbf{I})$ is independent of \mathbf{c} and ρ^t is the equivalent channel SNR. The output of η is the APP mean of \mathbf{c} based on \mathbf{r}^t in (4) and \mathcal{C} .

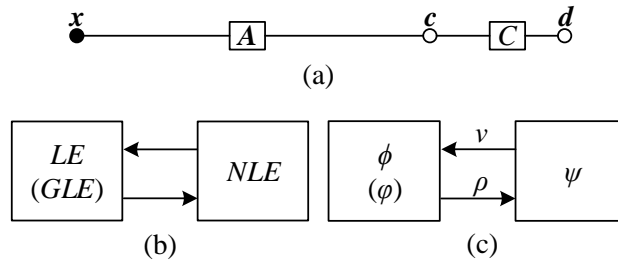


Fig. 1. Graphic illustrations for (a) compressed coding structure, (b) the receiver structure and (c) the SE recursion.

C. Evolution Analysis

The MSE performance of AMP in large system limits can be tracked by a scalar SE recursion [2], [3]. For the t -th iteration, let v^t be the *a priori* variance at the input of LE and ρ^t the *a priori* SNR at the input of NLE. Initializing with $v^1 = 1$, the SE recursion at the t -th iteration is given by [3]

$$\rho^t = \phi(v^t) \quad \text{and} \quad v^{t+1} = \psi(\rho^t), \quad (5)$$

where $\phi(v^t)$ gives the SNR at LE output and $\psi(\rho^t)$ gives the variance at DEC output. Fig. 1(c) illustrates the SE recursion.

The accuracy of SE was proved for AMP in [3]. The recent progress on AMP and its variants shows that the SE also holds for several non-separable denoisers [21]–[23]. The discussions in this paper are

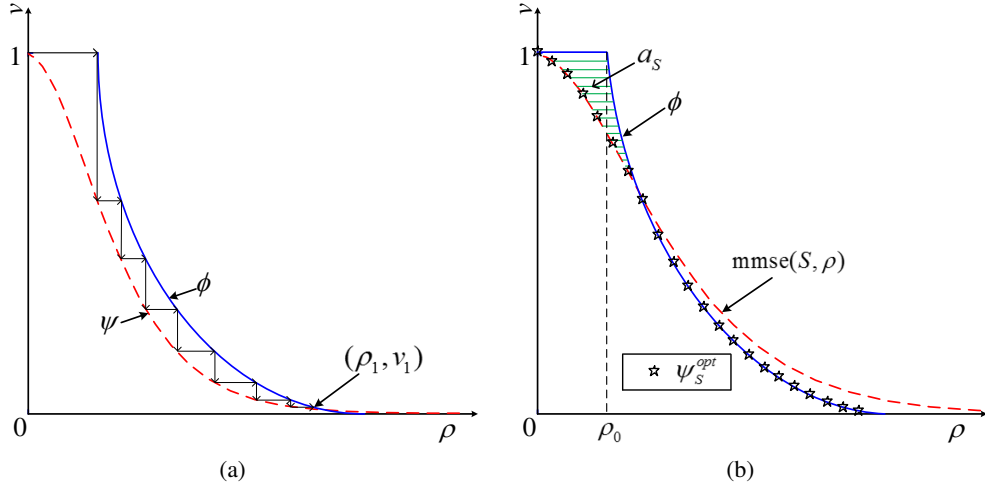


Fig. 2. Examples of the SE recursions with the same ϕ and different ψ .

based on the assumption that the SE holds for the AMP algorithm involving a DEC. Simulation results will be provided to support the assumption.

Fig. 2(a) shows an example of the SE recursion between ϕ and ψ , where the zigzag curve illustrates the iterative recovery trajectory. The fixed point is given by the first intersection of ϕ and ψ starting from $v = 1$, denoted as (ρ_1, v_1) . The final MSE is given by the variance of the fixed point, i.e., v_1 .

Property 1: Error-free decoding is achieved when $v_1 \rightarrow 0$, which requires $\psi(\rho) \leq \phi^{-1}(\rho)$ for $\rho \in [0, \infty)$ with $v = \phi^{-1}(\rho)$ being the inverse function of $\rho = \phi(v)$.

D. Area Property

According to [2], $\phi(v)$ in (5) is given by

$$\rho = \phi(v) = \frac{\delta}{v + \sigma^2}, \quad 0 \leq v \leq 1. \quad (6)$$

The capacity of a real-valued AWGN channel with Gaussian signaling is given by

$$C_G = 0.5 \log(1 + 1/\sigma^2). \quad (7)$$

From (6)–(7), we have the following lemma:

Lemma 1:

$$\frac{1}{2} \int_0^1 \phi(v) dv = \delta \cdot C_G. \quad (8)$$

The left hand side of (8) can be interpreted as the area under ϕ scaled by 0.5 for a real-valued channel. Lemma 1 bridges the area under ϕ and the AWGN channel capacity.

Assume that η for decoding \mathbf{c} is Bayes-optimal. Then $\psi(\rho)$ gives the minimum mean squared-error (MMSE) for estimating \mathbf{c} as

$$v = \psi(\rho) = \frac{1}{N} \cdot \mathbf{E} [\|\mathbf{c} - \mathbf{E}(\mathbf{c}|\mathbf{c} + \rho^{-1} \cdot \mathbf{w})\|^2], \quad (9)$$

where \mathbf{w} is independent of \mathbf{c} . The lemma below follows [24, Corollary 1]:

Lemma 2:

$$\frac{1}{2} \int_0^\infty \psi(\rho) \, d\rho = R_{\mathcal{C}}. \quad (10)$$

E. Achievable Rate

Define the inverse function of ϕ in (6) as

$$v = \phi^{-1}(\rho) = \begin{cases} 1, & 0 \leq \rho < \rho_0, \\ \frac{\delta}{\rho} - \sigma^2, & \rho \geq \rho_0, \end{cases} \quad (11)$$

where $\rho_0 \triangleq \frac{\delta}{1+\sigma^2}$ is shown in Fig. 2(b).

Let $\text{mmse}(\mathcal{S}, \rho)$ be the MMSE for detecting a symbol in \mathcal{S} from an AWGN channel with SNR ρ . Accordingly, denote ψ in (5) as $\psi_{\mathcal{S}}$ when \mathcal{S} is employed in \mathbf{c} . For an arbitrary underlying code \mathcal{C} , we have $\psi_{\mathcal{S}}(\rho) \leq \text{mmse}(\mathcal{S}, \rho)$ for $\rho \in [0, \infty)$. Combining with Property 1 yields

$$\psi_{\mathcal{S}}(\rho) \leq \min\{\phi^{-1}(\rho), \text{mmse}(\mathcal{S}, \rho)\}, \quad \rho \in [0, \infty). \quad (12)$$

According to Lemma 2, the achievable rate of \mathbf{c} can be maximized by maximizing the area under ψ . From (12), the maximal area is achieved when

$$\psi_{\mathcal{S}}^{\text{opt}}(\rho) = \min\{\phi^{-1}(\rho), \text{mmse}(\mathcal{S}, \rho)\}, \quad \rho \in [0, \infty). \quad (13)$$

Define

$$a_{\mathcal{S}} \triangleq \int_0^\infty (\phi^{-1}(\rho) - \psi_{\mathcal{S}}^{\text{opt}}(\rho)) \, d\rho. \quad (14)$$

Fig. 2(b) shows an example of $\psi_{\mathcal{S}}^{opt}(\rho)$ and $a_{\mathcal{S}}$ as illustrated by the star curve and the shadowed area, respectively. According to Lemmas 1–2, we have

$$a_{\mathcal{S}} = \int_0^1 \phi(v)dv - \int_0^\infty \psi_{\mathcal{S}}^{opt}(\rho)d\rho = 2\delta C_G - 2R_C. \quad (15)$$

The overall rate after the compression matrix is given by

$$R_{AC} = R_C/\delta = C_G - a_{\mathcal{S}}/2\delta. \quad (16)$$

Eq. (16) shows that the rate of a CC scheme is away from the AWGN capacity by a gap of $a_{\mathcal{S}}/2\delta$. In the next subsection, we show that this gap vanishes as $\delta, R_C \rightarrow 0$ with $R_{AC} = R_C/\delta$ fixed.

F. Approaching Capacity

We first consider the binary phase shift keying (BPSK) for \mathcal{S} . Afterwards, we extend the results to more general cases.

For BPSK, the entries of \mathbf{c} are drawn from $\mathcal{B} = \{+1, -1\}$ with equal probabilities. From (13), we have

$$\psi_{\mathcal{B}}^{opt}(\rho) = \min\{\phi^{-1}(\rho), \text{mmse}(\mathcal{B}, \rho)\}, \quad \rho \in [0, \infty), \quad (17)$$

where $\text{mmse}(\mathcal{B}, \rho)$ is the MMSE for detecting BPSK from an AWGN channel [25]:

$$\text{mmse}(\mathcal{B}, \rho) = 1 - \int_{-\infty}^{+\infty} \frac{e^{-x^2/2}}{\sqrt{2\pi}} \tanh(\rho - \sqrt{\rho}x) dx. \quad (18)$$

Following (14), we define

$$a_{\mathcal{B}} \triangleq \int_0^\infty (\phi^{-1}(\rho) - \psi_{\mathcal{B}}^{opt}(\rho)) d\rho. \quad (19)$$

The corresponding rate is given by

$$R_{AC} = C_G - a_{\mathcal{B}}/2\delta. \quad (20)$$

Theorem 1: Assume that the matching condition (17) holds for BPSK. Then, $R_{AC} \rightarrow C_G$ when $\delta, R_C \rightarrow 0$ with R_C/δ fixed.

Proof: See Appendix A. ■

Next, we consider a commonly used symmetric constellation \mathcal{S}_C such that if $s \in \mathcal{S}_C$ then $-s \in \mathcal{S}_C$. Such a \mathcal{S}_C includes quadrature phase shift keying (QPSK) and quadrature amplitude modulation (QAM) as special examples. For such \mathcal{S}_C , similar to (20), we can show that

$$R_{AC} = C_G - a_{\mathcal{S}_C}/2\delta, \quad (21)$$

where $a_{\mathcal{S}_C} = \int_0^\infty (\phi^{-1}(\rho) - \psi_{\mathcal{S}_C}^{opt}(\rho)) d\rho$ with the following matching condition

$$\psi_{\mathcal{S}_C}^{opt}(\rho) = \min\{\phi^{-1}(\rho), \text{mmse}(\mathcal{S}_C, \rho)\}, \quad \rho \in [0, \infty). \quad (22)$$

Theorem 2: Assume that the matching condition (22) holds for \mathcal{S}_C . Then, $R_{AC} \rightarrow C_G$ when $\delta, R_C \rightarrow 0$ with R_C/δ fixed.

Proof: Due to the symmetry, we can treat \mathcal{S}_C as the sum of multiple BPSK constellations multiplied by proper scalings. Recall the assumption that constellation points are drawn from \mathcal{S}_C with equal probability. According to [25, Proposition 14], we have $\text{mmse}(\mathcal{S}_C, \rho) \geq \text{mmse}(\mathcal{B}, \rho)$ for $\rho \in [0, \infty)$.

Comparing (17) and (22) yields $\psi_{\mathcal{S}_C}^{opt}(\rho) \geq \psi_{\mathcal{B}}^{opt}(\rho)$ for $\rho \in [0, \infty)$. Furthermore, we have $a_{\mathcal{S}_C} \leq a_{\mathcal{B}}$ according to $a_{\mathcal{S}}$ defined in (14). Recall Theorem 1 that $a_{\mathcal{B}}/2\delta \rightarrow 0$ when $\delta, R_C \rightarrow 0$ with R_C/δ fixed. Since $a_{\mathcal{S}_C} \leq a_{\mathcal{B}}$, $a_{\mathcal{S}_C}/2\delta \rightarrow 0$ also holds. From (21), we have $R_{AC} \rightarrow C_G$ and complete the proof. ■

Remark 1: Theorem 2 shows that R_{AC} of the CC scheme with \mathcal{S}_C can approach C_G under two conditions: (a) the matching condition (22) holds and (b) both R_C and $\delta \rightarrow 0$. These conditions require an underlying low-rate FEC code \mathcal{C} that meets the matching condition (22). In practice, it is a highly complicated task to design such a low-rate code (see [15]–[17] for details). There is another difficulty. Due to the Gaussian distribution of \mathbf{x} , the above CC scheme suffers from a high PAPR problem.

In what follows, we will address these two difficulties in the next two sections separately.

III. COMPRESSED CODING WITH CLIPPING

The aforementioned results are for the linear system $\mathbf{y} = \mathbf{A}\mathbf{c} + \mathbf{n}$. In this section, we extend the results to a more general system modeled below:

$$\mathbf{y} = f(\mathbf{x}) + \mathbf{n} = f(\mathbf{A}\mathbf{c}) + \mathbf{n}, \quad (23)$$

where f is a symbol-by-symbol function. This generalized CC scheme arises in various practical applications. An example is the clipping function for alleviating the high PAPR problem mentioned at the end of Section II that is given by

$$f(x) \triangleq \begin{cases} Z, & x > Z, \\ x, & -Z \leq x \leq Z, \\ -Z, & x < -Z, \end{cases} \quad (24)$$

where $Z > 0$ is the clipping threshold.

Alternatively, consider a slightly different system model:

$$\mathbf{y} = f(\mathbf{A}\mathbf{c} + \mathbf{n}). \quad (25)$$

As an example, f in (25) may represent the quantization effect of low-resolution analog-to-digital conversion on the received signal. In this section, we first focus on (23). The treatment for (25) is discussed in Appendix C-C.

A. GAMP and State Evolution

At the receiver side, generalized AMP (GAMP) can be used to recover \mathbf{c} from \mathbf{y} in (23) involving nonlinearity. Similar to AMP, the MSE performance of GAMP can be characterized by a SE recursion [26], [27]. We now briefly outline the GAMP algorithm and the corresponding SE recursion. Based on the SE, we analyze the achievable rate of GAMP for (23) following the procedure in Section II.

When $M, N \rightarrow \infty$ with $\delta = M/N$ fixed, we have $\|\mathbf{A}\|_F^2/M \rightarrow 1$ and $\|\mathbf{A}\|_F^2/N \rightarrow \delta$ since $A_{m,n} \sim \mathcal{N}(0, 1/N)$ (see (1)). Initializing $\hat{\mathbf{c}}^1 = \mathbf{0}$, $\mathbf{s}^0 = \mathbf{0}$ and $v^1 = 1$, the GAMP algorithm in [26] can be summarized by the following iteration between a generalized LE (GLE) and a NLE:

$$\text{GLE : } \hat{\mathbf{p}}^t = \mathbf{A}\hat{\mathbf{c}}^t - v^t \mathbf{s}^{t-1}, \quad (26a)$$

$$\mathbf{s}^t = \frac{g(\hat{\mathbf{p}}^t, \mathbf{y}) - \hat{\mathbf{p}}^t}{v^t}, \quad (26b)$$

$$\mathbf{r}^t = \hat{\mathbf{c}}^t + \frac{v^t/\delta}{1 - \langle \partial g(\hat{\mathbf{p}}^t, \mathbf{y}) / \partial \hat{\mathbf{p}}^t \rangle} \mathbf{A}^\top \mathbf{s}^t, \quad (26c)$$

$$\text{NLE : } \hat{\mathbf{c}}^{t+1} = \eta(\mathbf{r}^t), \quad (26d)$$

where $\langle \cdot \rangle$ denotes the average of the inputs. Fig. 1(b) illustrates the GAMP receiver. The final estimate is given by $\hat{\mathbf{c}}^{T+1}$, where T is the maximum number of iterations.

For GLE, $g(\hat{\mathbf{p}}^t, \mathbf{y})$ in (26b) performs the MMSE estimation of \mathbf{x} based on its prior $\hat{\mathbf{p}}^t$ and the observation \mathbf{y} in (23) as

$$g(\hat{p}_m^t, y_m) = \mathbb{E}[x_m | \hat{p}_m^t, y_m], \quad m = 1, 2, \dots, M, \quad (27)$$

where $p(\mathbf{x} | \hat{\mathbf{p}}^t) = \mathcal{N}(\hat{\mathbf{p}}^t, v^t \mathbf{I})$ at the t -th iteration. Similar to (4), \mathbf{r}^t in (26c) can be treated as an AWGN observation of \mathbf{c} as (4). For NLE, η is the same as (2b) in the AMP algorithm.

The MSE performance of GAMP in (26) can be tracked by an SE recursion [26], [27]. With abuse of notation, let v^t be the *a priori* variance at the input of GLE and ρ^t the *a priori* SNR at the input of NLE as shown in Fig. 1(c). Initializing with $v^1 = 1$, the SE recursion for (26) is given by [3], [26]

$$\rho^t = \varphi(v^t) \quad \text{and} \quad v^{t+1} = \psi(\rho^t), \quad (28)$$

where ψ is the same as (9), and φ is given as follows.

Let $p(x, \hat{p})$ be a joint Gaussian distribution as

$$\begin{bmatrix} x \\ \hat{p} \end{bmatrix} \sim \mathcal{N}(\mathbf{0}, \Sigma), \quad (29)$$

where

$$\Sigma = \begin{bmatrix} 1 & 1-v \\ 1-v & 1-v \end{bmatrix}. \quad (30)$$

Denote $p(y|x)$ as the likelihood of (23). According to [26], φ in (28) is given by

$$\rho = \varphi(v) = \frac{\delta}{v} \left(1 - \frac{\text{mmse}(x|\hat{p}, y)}{v} \right), \quad (31)$$

with

$$\text{mmse}(x|\hat{p}, y) \equiv \mathbb{E}[|x - \mathbb{E}(x|\hat{p}, y)|^2], \quad (32)$$

where the expectation is over $p(\hat{p}, x, y)$. The following result follows [26, Claim 1]:

Property 2: In (29)–(32), $\hat{p} \rightarrow x \rightarrow y$ forms a Markov chain. Thus, $p(\hat{p}, x, y) = p(y|x)p(x, \hat{p})$, where $p(y|x)$ and $p(x, \hat{p})$ are given by (23) and (29), respectively.

B. Area Property

The area properties derived below will be useful for achievable rate analyses in the next subsection.

Since ψ is still given by (9), Lemma 2 applies to ψ in (28). Theorem 3 below is presented first to underpin the area property of φ in Theorem 4.

Consider three random variables S_1, S_2, S_3 that form a Markov chain $S_1 \rightarrow S_2 \rightarrow S_3$. Assume that S_1 and S_2 are jointly distributed as

$$\begin{bmatrix} S_1 \\ S_2 \end{bmatrix} \sim \mathcal{N}(\mathbf{0}, \Sigma), \quad (33)$$

where Σ is given by (30). $S_2 \rightarrow S_3$ is characterized by a likelihood as $p(S_3|S_2)$. Denote the mutual information between S_1 and S_3 as $I(S_1; S_3)$ and define

$$\text{mmse}(S_2|S_1, S_3) \triangleq \mathbb{E}[|S_2 - \mathbb{E}(S_2|S_1, S_3)|^2], \quad (34)$$

where the expectation is over $p(S_1, S_2, S_3)$.

Theorem 3:

$$-\frac{\partial}{\partial v} I(S_1; S_3) = \frac{1}{2v} \left(1 - \frac{\text{mmse}(S_2|S_1, S_3)}{v} \right). \quad (35)$$

Proof: See Appendix B. ■

Denote $I(y; x)$ as the mutual information between y and x in (23), where $x \sim \mathcal{N}(0, 1)$. Theorem 4 below establishes an area property for φ .

Theorem 4:

$$\frac{1}{2} \int_0^1 \varphi(v) dv = \delta \cdot I(y; x). \quad (36)$$

Proof: According to Property 2, applying Theorem 3 to the Markov chain $\hat{p} \rightarrow x \rightarrow y$ yields

$$-\frac{\partial}{\partial v} I(\hat{p}; y) = \frac{1}{2v} \left(1 - \frac{\text{mmse}(x|\hat{p}, y)}{v} \right). \quad (37)$$

Taking integrations of the above equation yields

$$\frac{1}{2} \int_0^1 \frac{1}{v} \left(1 - \frac{\text{mmse}(x|\hat{p}, y)}{v} \right) dv = \int_0^1 -\frac{\partial}{\partial v} I(y; \hat{p}) dv \quad (38a)$$

$$= [I(y; \hat{p})]_{v=0} - [I(y; \hat{p})]_{v=1} \quad (38b)$$

$$\stackrel{(a)}{=} I(y; \hat{p} = x) - I(y; \hat{p} = 0) \quad (38c)$$

$$= I(y; x), \quad (38d)$$

where (a) is due to $p(\hat{p}, x)$ in (29)–(30). Comparing (38) and (31), it is clear to get (36), which completes the proof. \blacksquare

Remark 2: Beyond (23), Theorem 4 holds for general systems that can be modeled by $p(\mathbf{y}|\mathbf{x}) = \prod_{m=1}^M p(y_m|x_m)$, since the underlying proof of Theorem 3 does not specify $p(S_3|S_2)$. This can be seen from the proof of Theorem 4, where $p(S_3|S_2)$ characterizes the relationship between \mathbf{x} and \mathbf{y} in (23).

C. Achievable Rate

With the area properties of ψ and φ obtained in Lemma 2 and Theorem 4, respectively, we now evaluate the achievable rate of the generalized CC scheme according to the curve matching principle. The property below follows [28, Lemma 4.2].

Property 3: For $v \in [0, 1]$, $\varphi(v)$ is positive and decreasing with v .

From Property 3, $\rho = \varphi(v)$ is a one-to-one mapping from $v \in [0, 1]$. Following the definition of ϕ^{-1} in (11), we define the inverse function of $\rho = \varphi(v)$ as $v \equiv \varphi^{-1}(\rho)$ that is shown by the solid line in Fig. 3.

Assume a symmetrical constellation \mathcal{S}_C for \mathbf{c} . Similar to (12), ψ in GAMP is upper bounded by

$$\psi_f(\rho) \leq \min\{\varphi^{-1}(\rho), \text{mmse}(\mathcal{S}_C, \rho)\}, \quad \rho \in [0, \infty). \quad (39)$$

According to Lemma 2, the achievable rate of ψ can be maximized when the equality holds in (39), i.e.,

$$\psi_f^{\text{opt}}(\rho) = \min\{\varphi^{-1}(\rho), \text{mmse}(\mathcal{S}_C, \rho)\}, \quad \rho \in [0, \infty). \quad (40)$$

Based on (40), define

$$a_f \triangleq \int_0^\infty (\varphi^{-1}(\rho) - \psi_f^{\text{opt}}(\rho)) d\rho. \quad (41)$$

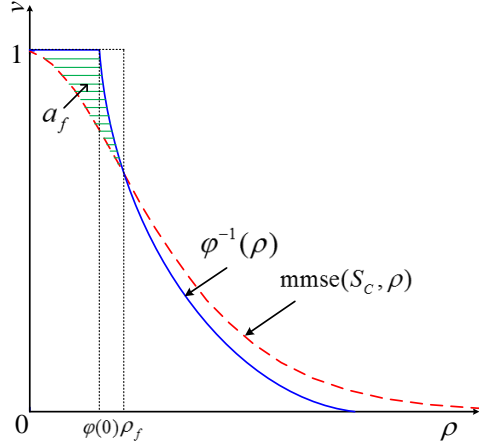


Fig. 3. Examples of transfer functions for GAMP.

Fig. 3 shows an example of a_f that is illustrated by the shadowed area. The maximal rate of ψ_f^{opt} in (40) after compression is given by

$$R_{AC} = \frac{1}{2\delta} \int_0^\infty \psi_f^{opt}(\rho) d\rho \quad (42)$$

Substituting (36) and (42) into (41) yields

$$a_f = 2\delta \cdot I(y; x) - 2\delta \cdot R_{AC} \Rightarrow R_{AC} = I(y; x) - a_f/2\delta. \quad (43)$$

The theorem below shows that the gap $a_f/2\delta$ vanishes when $\delta, R_C \rightarrow 0$ with R_C/δ fixed.

Theorem 5: Assume that the matching condition (40) holds for a symmetrical constellation \mathcal{S}_C . Then, $R_{AC} \rightarrow I(y; x)$ when $\delta, R_C \rightarrow 0$ with R_C/δ fixed.

Proof: See Appendix C-B. ■

Theorem 5 shows that R_{AC} of the generalized CC scheme with a practical \mathcal{S}_C can approach the mutual information between x and y in (23). To approach $I(y; x)$ in practice, a code should be designed to meet the matching condition (40) and meanwhile the code rate should be kept as low as possible. However, it is complicated to design a low-rate code to ensure (40) using curve matching [15]–[17]. The same obstacle happens to Theorem 2 as discussed in Remark 1. Indeed, Theorem 2 is a special case of Theorem 5 since $I(y; x) = C_G$ when f in (23) is removed. In the next section, we will treat this issue together.

IV. ANALOG SPATIAL COUPLING

In this section, ASC is introduced to avoid the difficulty in curve matching at low coding rates. This provides a simple method to approach capacity predicted by area properties using simple code structures [29] without complicated code optimizations [15], [16]. Incidentally, we will see in Section V-D that ASC-CC reveals a new multi-user scheme with short per-user block length and good performance.

A. ASC Principles

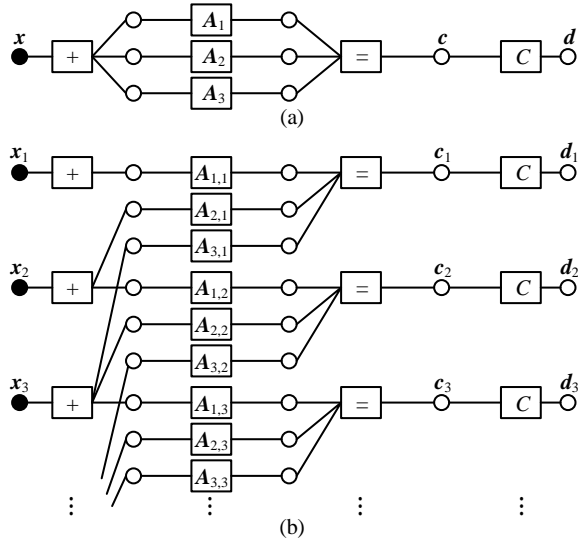


Fig. 4. (a) A modified version of Fig. 1(a) with $W = 3$. (b) An ASC-CC system based on (a) with $W = 3$. The addition is performed in the real domain.

Fig. 4(a) shows a slightly modified form of Fig. 1(a), in which c is repeated for W times ($W = 3$ in Fig. 4(a)). Each replica is multiplied by a compression matrix \mathbf{A}_i . The transmitted signal is

$$\mathbf{x} = (\mathbf{A}_1 + \mathbf{A}_2 + \cdots + \mathbf{A}_W)\mathbf{c}. \quad (44)$$

When the entries of \mathbf{A} and $\{\mathbf{A}_i\}$ are i.i.d. Gaussian distributed, Figs. 1(a) and 4(a) are equivalent by setting $\mathbf{A} = \mathbf{A}_1 + \mathbf{A}_2 + \cdots + \mathbf{A}_W$ after proper normalization.

Applying the analog spatial coupling principle [7], [8], [30] to K copies of Fig. 4(a), we obtain an analog spatially coupled compressed coding (ASC-CC) scheme in Fig. 4(b) [1], [14], [31]. For the j -th

($1 \leq j \leq K + W - 1$) copy, the transmitted signal is given by

$$\mathbf{x}_j = \frac{1}{W} \sum_{k=1}^K \mathbf{A}_{j+1-k,k} \mathbf{c}_k, \quad (45)$$

where $\{\mathbf{A}_{j+1-k,k}\}$ are assumed to be independent and the entries of each $\mathbf{A}_{j+1-k,k}$ have the same distribution as \mathbf{A} in (1). We assume the termination as $\mathbf{A}_{j+1-k,k} = \mathbf{0}$ for $j + 1 - k < 1$ or $j + 1 - k > W$. When K is large, we approximately have $E[x^2] = 1$ if we ignore the boundary effects for $j < W$ and $j > K$.

Consider transmitting \mathbf{x}_j over an AWGN channel as

$$\mathbf{y}_j = \mathbf{x}_j + \mathbf{n}_j = \frac{1}{W} \sum_{k=1}^K \mathbf{A}_{j+1-k,k} \mathbf{c}_k + \mathbf{n}_j, \quad (46)$$

where $j = 1, 2, \dots, K + W - 1$ and \mathbf{n}_j contains i.i.d. Gaussian noise. The AMP algorithm can be directly applied to the system in (46), of which the details can be found in [6], [28], [32].

B. State Evolution for the ASC-CC System

Compared with the SE in (5) for the CC system, SE for the ASC-CC system is a recursion between two vectors denoted as $\{v_j, j = 1, \dots, K + W - 1\}$ and $\{\rho_k, k = 1, \dots, K\}$. Initializing with $\{v_j^1 = 1, \forall j\}$, the vector SE given by [33, Definition 3.9] is equivalent to the following recursion

$$\rho_k^t = \frac{1}{W} \sum_{w=1}^W \phi(v_{k-1+w}^t), \quad \forall k, \quad (47a)$$

$$v_j^{t+1} = \frac{1}{W} \sum_{w=1}^W \psi(\rho_{j-W+w}^t), \quad \forall j, \quad (47b)$$

where $\rho_k^t = 0$ for $k < 1$ or $k > K$ due to the assumed termination. Functions $\phi(v)$ and $\psi(\rho)$ are the same as those in (5).

C. Potential Function Analysis

Following [34], we define the uncoupled potential function as²

$$U(v) = \int_{\phi(1)}^{\phi(v)} [\psi(\rho) - \phi^{-1}(\rho)] d\rho, \quad \text{for } v \in [0, 1]. \quad (48)$$

²Function $U(v)$ is defined based on the underlying CC system in Section II. The definition here differs from [34, Equation (4)] by an additive constant. Such difference does not affect the minimizer of $U(v)$.

Lemma 3: [34, Theorem 1] For the coupled recursion in (47), the variance of the fixed point is upper bounded by the minimizer of $U(v)$ when $K, W \rightarrow \infty$.

Here, we assume that $U(v)$ has a unique minimum. From Lemma 3, a sufficient condition for error-free decoding is that the minimizer of $U(v)$ tends to zero.

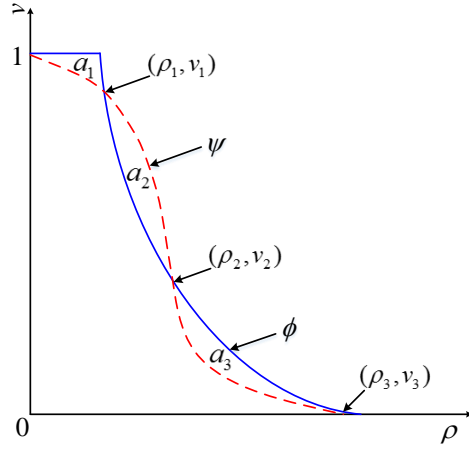


Fig. 5. An example of ϕ and ψ .

Fig. 5 shows an example of ϕ and ψ to illustrate Lemma 3. The two lines have three intersections as marked in Fig. 5, (ρ_i, v_i) , $i = 1, 2, 3$. In particular, one fixed point is at (ρ_3, v_3) with $v_3 \approx 0$. This implies error free decoding, which can only be treated as approximation. The areas a_1 , a_2 and a_3 marked in Fig. 5 are, respectively, calculated as

$$a_1 \equiv \int_{v_1}^1 [\phi(v) - \psi^{-1}(v)] dv, \quad (49a)$$

$$a_2 \equiv - \int_{v_2}^{v_1} [\phi(v) - \psi^{-1}(v)] dv, \quad (49b)$$

$$a_3 \equiv \int_{v_3}^{v_2} [\phi(v) - \psi^{-1}(v)] dv. \quad (49c)$$

It can be verified that the minimizer of $U(v)$ is either v_1 or v_3 . The critical point is $U(v_1) = U(v_3)$, or equivalently,

$$a_2 = a_3. \quad (50)$$

According to Lemma 2 and (49), we have from Fig. 5

$$R_C = \frac{1}{2} \int_0^\infty \psi(\rho) d\rho = \frac{1}{2} \left\{ \int_0^1 \phi(v) dv - a_1 + a_2 - a_3 \right\}. \quad (51)$$

When the critical point (50) is reached, the achievable rate R_{AC} is given by

$$R_{AC} = \frac{R_C}{\delta} = \frac{1}{2\delta} \left\{ \int_0^1 \phi(v) dv - a_1 \right\} = C_G - a_1/2\delta, \quad (52)$$

where the termination effects are ignored.

Comparing (52) with (16), we can see that the achievable rate of the ASC-CC scheme is very similar to the CC scheme. Following the procedure in Section II-F, we can show that $R_{ASC} \rightarrow C_G$ when $R_C, \delta \rightarrow 0$ with their ratio fixed. Note that the CC scheme requires that the matching condition holds while the ASC-CC scheme does not, which provides a simple way to avoid the difficulty of low rate code design.

V. SIMULATION RESULTS

A. ASC-CC with a Low Rate Underlying Code

The dashed lines in Fig. 6 show the bit error rate (BER) performance of an ASC-CC scheme. A concatenated zigzag Hadamard (CZH) code (non-systematic and un-punctured) with BPSK modulation is used for c with two component codes [29]. The Hadamard code length is 64, the number of information bits (per copy) is 24576 and $R_C = 3/64$. Recall that the theoretical analysis of ASC in Section IV-C requires $K, W \rightarrow \infty$. But, large K and W incur increased complexity. In Fig. 6, we set $K = 50$ and $W = 3$.

For complexity considerations, each $\mathbf{A}_{j,k}$ is generated using randomly selected rows from an $N \times N$ Hadamard matrix. The difference between Hadamard and i.i.d. Gaussian sensing matrices involving SC has been analyzed in [35]. We observed that this difference is typically very small for ASC-CC. Fast Hadamard transform (FHT) is used with complexity $\log_2(N)$ per bit. Soft output FHT [29] is used for decoding the CZH code. Iteration proceeds until convergence.

Theoretically, the AMP algorithm requires asymptotically large sensing matrices, which incurs high cost even with FHT. Simulations show that the performance of the above scheme remains almost unchanged

for $N > 65536$. Therefore, to reduce cost, each copy (coded length = 524288) is partitioned into 8 parts, each of length 65536, that are individually compressed.

In Fig. 6, we consider two rate cases: $R_{AC} = 0.5$ and $R_{AC} = 1$. Termination incurs rate loss in ASC and the actual rate realized by ASC-CC is given by $R_{ASC} \equiv R_{AC} \cdot K / (K + W - 1)$ [7]. For ASC with $W = 3$ and $K = 50$, $R_{ASC} = 0.4808$ and 0.9615 in Fig. 6. At $R_{ASC} = 0.9615$, BER falls sharply when SNR passes the threshold. At $R_{ASC} = 0.4808$, BER falls slowly. At $R_{ASC} = 0.9615$, the performance of ASC-CC surpasses the corresponding SNR threshold for BPSK signaling (7.37 dB) and is only 0.65 dB away from the Gaussian capacity threshold. Clearly, ASC-CC offers the shaping gain required to approach Gaussian capacity.

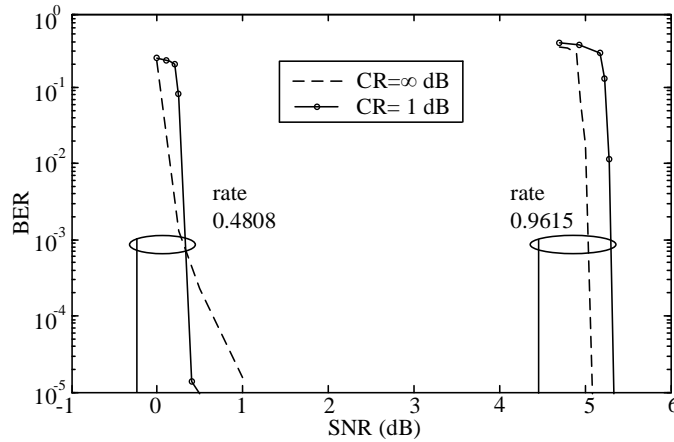


Fig. 6. Simulation results for ASC-CC systems. The vertical lines represent the SNR thresholds for Gaussian capacity. $CR = \infty$ dB represents the linear system without clipping.

B. Clipping Effects on ASC-CC

We consider the following clipped ASC-CC system

$$\mathbf{y}_j = \alpha \cdot \text{clip}(\mathbf{x}_j) + \mathbf{n}_j, \quad j = 1, 2, \dots, K + W - 1, \quad (53)$$

where $\text{clip}(\cdot)$ and $\{\mathbf{x}_j, \forall j\}$ are given by (24) and (45), respectively. The coefficient $\alpha \triangleq \sqrt{1/E[|\text{clip}(x)|^2]}$ normalizes the transmit power to unit. Define the clipping ratio (CR) as $CR \triangleq 10 \log_{10}(Z^2/E[x^2])$. When $CR = \infty$ dB, we have $\alpha = 1$ and (53) reduces to the linear ASC-CC system in Section V-A.

The solid lines in Fig. 6 with circles show the BER performance of the ASC-CC system with clipping, where settings are the same as those in Section V-A. We can see that clipping causes performance loss at

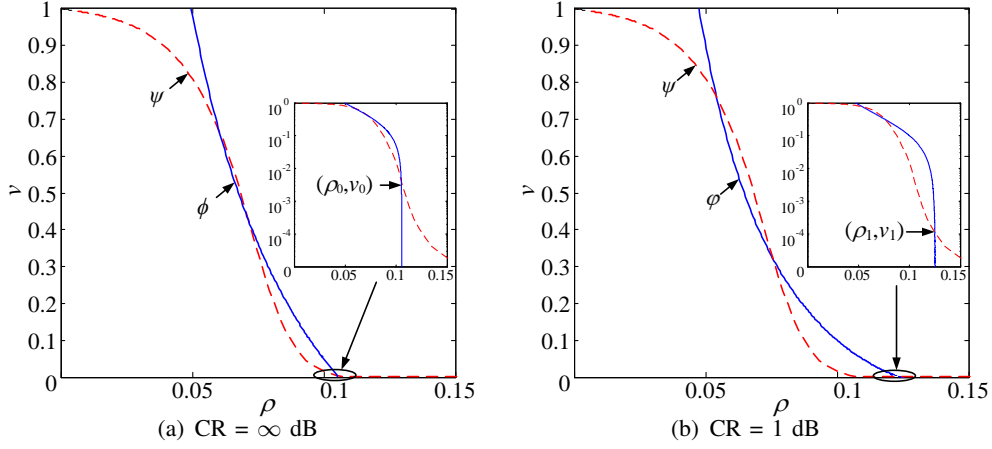


Fig. 7. Examples of transfer functions. $R_{\text{ASC}} = 0.4808$ and $\text{SNR} = 0.5$ dB.

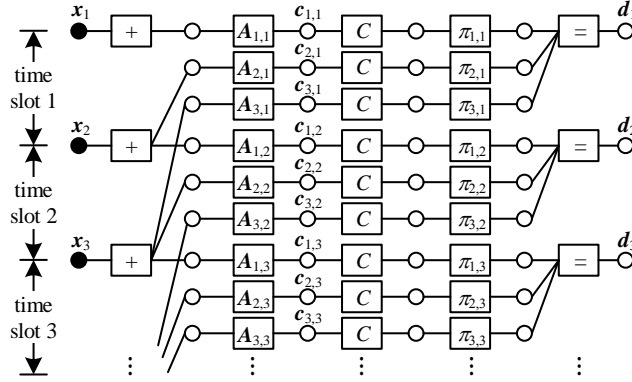


Fig. 8. A modified ASC-CC scheme of Fig. 4(c) with $W = 3$, where $\{\pi_{j,k}\}$ denote different interleaves.

$R_{\text{ASC}} = 0.9615$, but interestingly, improves performance at $R_{\text{ASC}} = 0.4808$ at low BERs. Similar results have been reported in [31]. An intuitive explanation based on the SE analysis is given as follows.

Fig. 7 plots transfer functions at $R_{\text{ASC}} = 0.4808$ and $\text{SNR} = 0.5$ dB in Fig. 6 for $\text{CR} = \infty$ dB and $\text{CR} = 1$ dB separately. It can be verified that the minimizers of the potential function for $\text{CR} = \infty$ dB and $\text{CR} = 1$ dB are given by (ρ_0, v_0) and (ρ_1, v_1) , respectively, which are highlighted in sub-figures of Fig. 7. Since $v_1 \ll v_0$, the final MSE performance for $\text{CR} = 1$ dB is better than that of $\text{CR} = \infty$ dB. For more insights, it can be observed that φ for $\text{CR} = 1$ dB has lower slope than ϕ for $\text{CR} = \infty$ dB at small v , which results in a better matching condition between ϕ and ψ and hence improves the performance.

C. Modified ASC-CC Schemes

Fig. 8 shows a modified version of Fig. 4(b), in which each input \mathbf{d}_k is, after independent interleaving, encoded for W times. Fig. 8 reduces to Fig. 4(b) if all interleavers $\{\pi_{j,k}\}$ are the same, as then all $\{\mathbf{c}_{j,k}\}$ are the same for a copy. Thus Figs. 8 and 4(b) differ only in interleaving. If the random connection technique in [7] is applied to Fig. 8, the W component codes for each copy can be combined to form an overall concatenated code. Then Fig. 8 is equivalent to Fig. 4(b). We observed that the structural connection in Fig. 8 leads to performance improvement in some situations. The extra interleaving in Fig. 8 offers more randomness, which intuitively is beneficial to performance. However, so far, we are unable to provide analytical explanations.

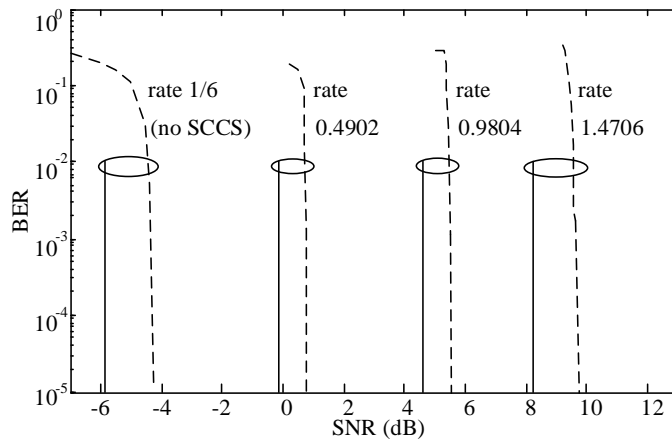


Fig. 9. Performance of the modified ASC-CC system.

Fig. 9 shows the BER performance of the modified ASC-CC system using a rate-1/2 non-systematic and un-punctured zigzag Hadamard (ZH) code [29] with Hadamard code length = 4 and number of information bits per copy = 16384. The rate of the CZH code = 1/6. Each copy is partitioned into 3 parts that are individually compressed. The sensing matrices are based on a size $N_H = 32768$ Hadamard matrix. For ASC, $W = 3$ and $K = 100$.

We call this ASC-CC scheme as a master code. We can puncture this master code to obtain different rates. Fig. 9 shows the simulation results for $R_{ASC} = 0.4902, 0.9804$ and 1.4706 , where random puncturing is used. The non-puncturing rate is 1/6. From Fig. 9, we can see that this master code is universal since it can be randomly punctured without affecting the relative performance measured by the gaps toward

capacity. At $R_{\text{ASC}} = 0.4902$, nearly error-free performance is achieved at only 0.7 dB away from the theoretical limit for Gaussian signaling. Such universal codes have been widely discussed for various applications, such as type-II ARQ [19], [20] and distributed caching systems [36].

D. A Multiuser ASC-CC System with Short Block Length per User

We now consider the application of ASC-CC in a multi-user system of K users. The overall system structure is the same as that in Fig. 8 except that $\{\mathbf{d}_k\}$ are generated separately by K users. The transmitted signals from K users are encoded and transmitted in a decentralized way without information sharing except for proper transmission time scheduling. Specifically, we divide the time span into slots, each of which corresponds to a copy. In slot k , user k generates the signals based on its data \mathbf{d}_k and transmits them over W slots starting from k . The signals from different users are separated by user-specific interleaving, following the interleave division multiple access (IDMA) principle [37]. At the receiver, the signals from K users are naturally combined, which has the same effect as a linear summation in Fig. 8 [12].

In general, to achieve improved performance, a spatially-coupled LDPC code requires much longer block length than the underlying LDPC code before coupling [8], [30]. This is because the former involves multiple copies of the latter. In a multiuser ASC-CC system, the increased overall block length is shared by multiple users. This achieves the benefit of spatial coupling without increasing the codeword length of each user.

Incidentally, the block length problem is usually due to the latency constraint. It cannot be solved by, e.g., increasing processing speed. It is a source problem, and in many real-time applications, the source can only generate a limited number of information bits within a fixed duration. The scheme below is to fill this fixed duration with the signals from multiple users, which effectively increases block length.

Fig. 10 shows the performance of the ASC-CC-IDMA scheme for both $K = 16$ and 64 using a rate-1/4 non-systematic and un-punctured ZH code. To achieve a rate exactly $R_{\text{AC}} = 0.5$, for $K = 16$, each $\mathbf{A}_{j,w}$ is formed by randomly selecting 1725 rows in an Hadamard matrix with $N_H = 4096$ so $\delta = 0.4211$; for $K = 64$, each $\mathbf{A}_{j,w}$ is formed by randomly selecting 1956 rows in an Hadamard matrix with $N_H = 4096$ so $\delta = 0.4775$. For ASC, $W = 4$. The ASC-CC performance improves with K . This is a common property

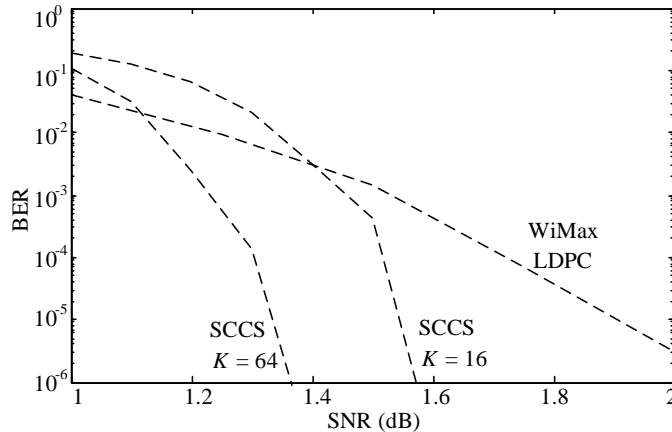


Fig. 10. Multiuser performance of the modified ASC-CC scheme and the WiMax LDPC code [38]. All schemes have a coding rate 0.5 in real channels.

of ASC [8], since the overhead due to termination reduces when K increases.

The performance of the rate-1/2 LDPC code for the WiMax standard [38] with 1152 information bits is compared in Fig. 10, for which users are separated by TDMA. We can see that ASC-CC outperforms the conventional LDPC coded TDMA scheme noticeably. Intuitively, the coding rate of each user in ASC-CC is 1/8 (after compression) since it occupies $W = 4$ slots. This is much lower than the rate ($= 1/2$) of the LDPC code. Therefore, ASC-CC might provide better coding gain if cross user interference can be ignored. However, interference does exist in ASC-CC. It appears that ASC-CC provides an efficient way for multiuser interference cancelation. This phenomenon was first noted in [39] for LDPC codes with SC but without compression.

CDMA with conventional successive interference cancelation (SIC) cannot help in this case. If a short code is used by each user in CDMA, decoding loss will accumulate in SIC, resulting in large overall loss. Superposition coding [40] also suffers from the same problem. Clearly, ASC-CC offers an attractive solution to the latency problem by sharing a long block length by multiple users in multi-user systems.

VI. CONCLUSIONS

In this paper, we proposed a CC scheme that combines CS with FEC coding, where AMP is used for decoding. We derived the performance limit of the CC scheme and showed that CC can asymptotically approach Gaussian capacity. This capacity approaching property can be maintained in systems with non-

linear effects such as clipping and quantization. We also studied an ASC-CC scheme to circumvent the difficulty in optimizing low-rate codes for approaching capacity in the CC scheme. We showed that ASC-CC can maintain universally good performance under random puncturing. By sharing the overall code length among multiple users, ASC-CC also relieves the requirement on per-user block length to achieve good performance in multi-user environments. The above claims are supported by extensive theoretical and numerical results.

APPENDIX A

PROOF OF THEOREM 1

It can be verified that $\text{mmse}(\mathcal{B}, \rho) = \phi^{-1}(\rho)$ has exactly one solution for $\rho \in [0, \infty)$, which is denoted as $\rho_{\mathcal{B}}$. Recalling $\rho = \phi(v) = \frac{\delta}{v + \sigma^2}$, we have $\rho \rightarrow 0$ as $\delta \rightarrow 0$. Apply Taylor expansion to $\text{mmse}(\mathcal{B}, \rho)$ in (18) at $\rho = 0$ as [25]

$$v = \text{mmse}(\mathcal{B}, \rho) = 1 - \rho + o(\rho). \quad (54)$$

Substituting (54) into $\phi(v)$ yields

$$\rho_{\mathcal{B}} = \frac{\delta}{1 - \rho_{\mathcal{B}} + \sigma^2} \iff \rho_{\mathcal{B}}^2 - (1 + \sigma^2)\rho_{\mathcal{B}} = -\delta \quad (55a)$$

$$\iff \left(\rho_{\mathcal{B}} - \frac{1 + \sigma^2}{2} \right)^2 = \left(\frac{1 + \sigma^2}{2} \right)^2 - \delta \quad (55b)$$

$$\stackrel{(a)}{\iff} \rho_{\mathcal{B}} = \frac{1 + \sigma^2}{2} - \sqrt{\left(\frac{1 + \sigma^2}{2} \right)^2 - \delta}, \quad (55c)$$

where (a) is due to that we consider the solution at the vicinity of $\rho = 0$ and the other solution (a larger value) is abandoned.

According to (17), we have

$$\psi_{\mathcal{B}}^{\text{opt}}(\rho) = \begin{cases} \text{mmse}(\mathcal{B}, \rho), & 0 \leq x \leq \rho_{\mathcal{B}}, \\ \phi^{-1}(\rho), & \rho_{\mathcal{B}} < x. \end{cases} \quad (56)$$

For $a_{\mathcal{B}}$ in (19), it can be shown from (56) that

$$a_{\mathcal{B}} = \int_0^{\rho_{\mathcal{B}}} (\phi^{-1}(\rho) - \text{mmse}(\mathcal{B}, \rho)) d\rho \leq \int_0^{\rho_{\mathcal{B}}} (1 - \text{mmse}(\mathcal{B}, \rho)) d\rho. \quad (57)$$

Combining (57) and (54) yields

$$a_{\mathcal{B}} \leq \int_0^{\rho_{\mathcal{B}}} (\rho + o(\rho)) d\rho = 0.5\rho_{\mathcal{B}}^2 + o(\rho_{\mathcal{B}}^2). \quad (58)$$

In (55c), we treat $\rho_{\mathcal{B}}$ as a function of δ and apply Taylor expansion at $\delta = 0$ as

$$\rho_{\mathcal{B}} = \frac{\delta}{1 + \sigma^2} + o(\delta). \quad (59)$$

Substituting (59) into (58), we have

$$\frac{a_{\mathcal{B}}}{2\delta} \leq 0.25 \frac{\delta}{(1 + \sigma^2)^2} + o(\delta). \quad (60)$$

As $\delta \rightarrow 0$, we can see from (60) that $a_{\mathcal{B}}/2\delta \rightarrow 0$, and therefore complete the proof.

APPENDIX B

PROOF OF THEOREM 3

Start with evaluating $I(S_1; S_3)$ as

$$I(S_1; S_2, S_3) = I(S_1; S_3, S_2) \stackrel{(a)}{\iff} I(S_1; S_3) + I(S_1; S_2|S_3) = I(S_1; S_2) + I(S_1; S_3|S_2) \quad (61a)$$

$$\stackrel{(b)}{\iff} I(S_1; S_3) = I(S_1; S_2) - I(S_1; S_2|S_3). \quad (61b)$$

In (61a), we simply rearrange the variables. In (a), we apply the chain rule of the conditional mutual information. In (b), we apply the property of Markov chain, i.e., $I(S_1; S_3|S_2) = 0$. From (61b), we evaluate $I(S_1; S_2)$ and $I(S_1; S_2|S_3)$ separately as follows.

Based on interpretation in [25], S_1 and S_3 can be viewed as two independent observations for S_2 . In particular, S_1 is an AWGN observation of S_2 according to (33) and (30). From [25], we have $I(S_1; S_2) = 0.5\log(1 + \rho)$ with ρ being the effective SNR of the AWGN channel. Following the mutual information and MMSE identity for AWGN channel with side information, we have [25]

$$I(S_1; S_2|S_3 = s_3) = \frac{1}{2} \int_0^{\rho} \text{mmse}(\rho, S_2|S_3 = s_3) d\rho, \quad (62)$$

where s_3 is a realization of S_3 and $\text{mmse}(\rho, S_2|S_3 = s_3)$ represents the minimum MSE of estimating S_2 from the AWGN observation S_1 with side information $S_3 = s_3$. Taking expectation of $I(S_1; S_2|S_3 = s_3)$ with respect to (w.r.t.) S_3 yields

$$I(S_1; S_2|S_3) = \mathbb{E}[I(S_1; S_2|S_3 = s_3)] = \frac{1}{2} \int_0^\rho \mathbb{E}[\text{mmse}(\rho, S_2|S_3 = s_3)] d\rho = \frac{1}{2} \int_0^\rho \text{mmse}(\rho, S_2|S_3) d\rho. \quad (63)$$

For (61b), we substitute $I(S_1; S_2)$ and $I(S_1; S_2|S_3)$ and yield

$$I(S_3; S_1) = \frac{1}{2} \log(1 + \rho) - \frac{1}{2} \int_0^\rho \text{mmse}(\rho, S_2|S_3) d\rho. \quad (64)$$

Note that $\text{mmse}(\rho, S_2|S_3)$ in (64) is a function of the effective SNR ρ . Taking partial derivative of $I(S_3; S_1)$ w.r.t. ρ in (64) yields

$$\frac{\partial}{\partial \rho} I(S_3; S_1) = \frac{\partial}{\partial \rho} \left[\frac{1}{2} \log(1 + \rho) - \frac{1}{2} \int_0^\rho \text{mmse}(\rho, S_2|S_3) d\rho \right] = \frac{1}{2(1 + \rho)} - \frac{1}{2} \text{mmse}(\rho, S_2|S_3). \quad (65)$$

Next, the effective SNR ρ should be identified for the effective AWGN channel. According to (33) and (30), $p(S_1, S_2)$ is given by

$$p(S_2, S_1) \propto \exp \left(-\frac{1}{2} [S_2, S_1] \Sigma^{-1} [S_2, S_1]^T \right) \propto \exp \left[-\frac{1}{2} \left(\frac{S_1^2}{v(1-v)} - \frac{2}{v} S_2 S_1 + \frac{S_2^2}{v} \right) \right]. \quad (66)$$

According to Bayes' rule, $p(S_1|S_2)$ is given by

$$p(S_1|S_2) = \frac{p(S_2, S_1)}{p(S_2)} \propto \frac{\exp \left[-\frac{1}{2} \left(\frac{1}{v(1-v)} S_1^2 - \frac{2}{v} S_2 S_1 + \frac{1}{v} S_2^2 \right) \right]}{\exp \left[-\frac{S_2^2}{2} \right]} \quad (67a)$$

$$\propto \exp \left[-\frac{1}{2} \left(\frac{S_1^2}{v(1-v)} - \frac{2}{v} S_2 S_1 + \frac{1-v}{v} S_2^2 \right) \right] \quad (67b)$$

$$\propto \exp \left[-\frac{S_1^2 - 2(1-v)S_2 S_1 + (1-v)^2 S_2^2}{2v(1-v)} \right] \quad (67c)$$

$$\propto \exp \left[-\frac{(S_1 - (1-v)S_2)^2}{2v(1-v)} \right]. \quad (67d)$$

The conditional distribution of $p(S_1|S_2)$ is given by

$$p(S_1|S_2) = \mathcal{N}(S_1; (1-v)S_2, v(1-v)). \quad (68)$$

Eq. (68) is equivalent to the following AWGN channel

$$S_1 = (1-v) \cdot S_2 + \mathcal{N}(0, v(1-v)), \quad (69)$$

where the noise is independent of S_2 . The effective SNR ρ is given by

$$\rho = \frac{(1-v)^2}{v(1-v)} \Leftrightarrow v = \frac{1}{1+\rho}. \quad (70)$$

Substituting $v = \frac{1}{1+\rho}$ into (65) yields

$$-\frac{\partial}{\partial v} I(S_3; S_1) = \left[-\frac{\partial}{\partial \rho} I(S_3; S_1) \right]_{\rho=\frac{1-v}{v}} \cdot \frac{d}{dv} \rho \quad (71a)$$

$$= \left(\frac{1}{2(1+\rho)} - \frac{\text{mmse}(\rho, S_2|S_3)}{2} \right)_{\rho=\frac{1-v}{v}} \cdot \left(\frac{1}{v^2} \right) \quad (71b)$$

$$= \frac{1}{2} [v - \text{mmse}(S_2|S_1, S_3)] \cdot \frac{1}{v^2} \quad (71c)$$

$$= \frac{1}{2v} \left(1 - \frac{\text{mmse}(S_2|S_1, S_3)}{v} \right). \quad (71d)$$

Therefore,

$$-\frac{\partial}{\partial v} I(S_3; S_1) = \frac{1}{2v} \left(1 - \frac{\text{mmse}(S_2|S_1, S_3)}{v} \right), \quad (72)$$

which completes the proof of Theorem 3.

APPENDIX C

A. An Upper Bound of $\varphi(v)$

For $\mathbf{y} = f(\mathbf{x}) + \mathbf{n}$, we assume that f does not change the average power of \mathbf{x} , i.e., $\mathbb{E}[|f(x)|^2] = \mathbb{E}[|x|^2]$.

The following proposition gives an upper bound of φ .

Proposition 1: For $v \in [0, 1]$, $\rho = \varphi(v)$ in (31) is upper bounded by $\delta \cdot \left(\frac{1+\sigma^2}{4\sigma^2} \right)$.

Proof: Define $\mathbf{z} = f(\mathbf{x})$ and $\text{mmse}(z|y)$ as the minimum MSE of estimating \mathbf{z} from $\mathbf{y} = \mathbf{z} + \mathbf{n}$. Note that $\mathbb{E}[|f(x)|^2] = 1$. According to [25], $\text{mmse}(z|y) \geq \frac{1}{1+1/\sigma^2}$. According to the data processing inequality, it is clear that $\text{mmse}(x|y) \geq \text{mmse}(z|y)$.

Rewrite $\varphi(v)$ in (31) as

$$\rho = \varphi(v) = \delta \left(v + \frac{1}{\frac{1}{\text{mmse}(x|\hat{p}, y)} - \frac{1}{v}} \right)^{-1}. \quad (73)$$

Combining $\text{mmse}(x|y) \geq \frac{1}{1+1/\sigma^2}$ with (73) yields

$$\rho \leq \delta \left(v + \frac{1}{1 + 1/\sigma^2 - \frac{1}{v}} \right)^{-1} = \delta \left(\frac{1 + 1/\sigma^2 - \frac{1}{v}}{v(1 + 1/\sigma^2)} \right) \quad (74a)$$

$$= \delta \left(-\frac{\sigma^2}{1 + \sigma^2} \cdot \frac{1}{v^2} + \frac{1}{v} \right) \quad (74b)$$

$$= \delta \left(-\frac{\sigma^2}{1 + \sigma^2} \left(\frac{1}{v} - \frac{1 + \sigma^2}{2\sigma^2} \right)^2 + \frac{1 + \sigma^2}{4\sigma^2} \right) \quad (74c)$$

$$\leq \delta \left(\frac{1 + \sigma^2}{4\sigma^2} \right), \quad (74d)$$

which completes the proof. ■

B. Proof of Theorem 5

First, we prove that $R_{AC} \rightarrow I(y; x)$ as $\delta, R_C \rightarrow 0$ with R_C/δ fixed for the BPSK case as follows.

Recall $\rho = \varphi(v)$ in (31) as

$$\rho = \varphi(v) = \frac{\delta}{v} \left(1 - \frac{\text{mmse}(x|\hat{p}, y)}{v} \right) \leq \frac{\delta}{v}. \quad (75)$$

From Proposition 1, we can see that $\rho \rightarrow 0$ as $\delta \rightarrow 0$. Then, we apply Taylor expansion to $\text{mmse}(\mathcal{B}, \rho)$ at $\rho = 0$ as [25]

$$v = \text{mmse}(\mathcal{B}, \rho) = 1 - \rho + o(\rho). \quad (76)$$

Denote ρ_f as solutions of $\varphi^{-1}(\rho) = \text{mmse}(\mathcal{B}, \rho)$. Combining (75) and (76), we have ρ_f at the vicinity of $\rho = 0$

$$\rho_f \leq \frac{\delta}{1 - \rho_f} \xrightarrow{(a)} \left(\rho_f - \frac{1}{2} \right)^2 \leq \frac{1}{4} - \delta \xrightarrow{(b)} 0 \leq \rho_f \leq \frac{1}{2} - \sqrt{\frac{1}{4} - \delta}, \quad (77)$$

where (a) and (b) are due to that $\delta \rightarrow 0$ and $\rho \rightarrow 0$. Define $\rho_f^{max} \triangleq \frac{1}{2} - \sqrt{\frac{1}{4} - \delta}$. From (41), we have

$$a_f \leq \int_0^{\rho_f} (1 - \text{mmse}(\mathcal{B}, \rho)) d\rho \leq \int_0^{\rho_f^{max}} (1 - \text{mmse}(\mathcal{B}, \rho)) d\rho \triangleq a_f^{max}. \quad (78)$$

Following (55c) and (58)–(60), we can show $\frac{(a_f^{max})^2}{2\delta} \rightarrow 0$ as $\delta \rightarrow 0$. Since $a_f \leq a_f^{max}$, we have $a_f/2\delta \rightarrow 0$ as $\delta \rightarrow 0$, which completes the proof for the BPSK case.

Following the same method in the proof of Theorem 2, the above result can be extended to a general symmetrical constellation \mathcal{S}_C .

C. Extension of Theorem 5

The proof of Theorem 5 relies on Proposition 1 to show that ρ is in the vicinity of zero when $\delta \rightarrow 0$. In fact, Theorem 5 holds for an arbitrary signal model as long as Proposition 1 holds. Another provable example is $\mathbf{y} = f(\mathbf{x} + \mathbf{n})$. When f is a one-to-one mapping function, it can be shown that $\text{mmse}(x|\hat{p}, y) = \frac{v\sigma^2}{v+\sigma^2}$, which is the MMSE for $\mathbf{y} = \mathbf{x} + \mathbf{n}$. When f is a many-to-one mapping function, we have $\text{mmse}(x|\hat{p}, y) > \frac{v\sigma^2}{v+\sigma^2}$ due to the ambiguity from \mathbf{y} to $\mathbf{x} + \mathbf{n}$. Thus, we have

$$\text{mmse}(x|\hat{p}, y) \geq \frac{v\sigma^2}{v + \sigma^2}. \quad (79)$$

Combining (79) and (73) yields

$$\rho = \varphi(v) \leq \delta \left(v + \frac{1}{\frac{v+\sigma^2}{v\sigma^2} - \frac{1}{v}} \right)^{-1} \leq \frac{\delta}{v + \sigma^2} \leq \frac{\delta}{\sigma^2}. \quad (80)$$

It is clear that $\rho \rightarrow 0$ as $\delta \rightarrow 0$.

REFERENCES

- [1] C. Liang, J. Ma, and L. Ping, "Towards Gaussian capacity, universality and short block length," *Proc. 9th Int. Symp. Turbo Codes (ISTC)*, pp. 412–416, Sep 2016.
- [2] D. L. Donoho, A. Maleki, and A. Montanari, "Message-passing algorithms for compressed sensing," in *Proc. Nat. Acad. Sci.*, vol. 106, no. 45, Nov. 2009, pp. 18 914–18 919.
- [3] M. Bayati and A. Montanari, "The dynamics of message passing on dense graphs, with applications to compressed sensing," *IEEE Trans. Inf. Theory*, vol. 57, no. 2, pp. 764–785, Feb 2011.
- [4] J. Ma, L. Liu, X. Yuan, and L. Ping, "On orthogonal amp in coded linear vector systems," *IEEE Transactions on Wireless Communications*, vol. 18, no. 12, pp. 5658–5672, Dec 2019.
- [5] C. Rush, A. Greig, and R. Venkataramanan, "Capacity-achieving sparse superposition codes via approximate message passing decoding," *IEEE Trans. Inf. Theory*, vol. 63, no. 3, pp. 1476–1500, Mar 2017.
- [6] J. Barbier and F. Krzakala, "Approximate message-passing decoder and capacity achieving sparse superposition codes," *IEEE Trans. Inf. Theory*, vol. 63, no. 8, pp. 4894–4927, Aug 2017.
- [7] S. Kudekar, T. Richardson, and R. L. Urbanke, "Spatially coupled ensembles universally achieve capacity under belief propagation," *IEEE Trans. Inf. Theory*, vol. 59, no. 12, pp. 7761–7813, Dec. 2013.
- [8] D. G. M. Mitchell, M. Lentmaier, and D. J. Costello, Jr., "Spatially coupled LDPC codes constructed from protographs," *IEEE Trans. Inf. Theory*, vol. 61, no. 9, pp. 4866–4889, Sep. 2015.
- [9] X. Ma, C. Liang, K. Huang, and Q. Zhuang, "Block Markov superposition transmission: Construction of big convolutional codes from short codes," *IEEE Trans. Inf. Theory*, vol. 61, no. 6, pp. 3150–3163, Jun. 2015.

- [10] W. Hou, S. Lu, and J. Cheng, "Spatially coupled repeater-combiner-convolutional codes," *IEEE Commun. Lett.*, vol. 20, no. 1, pp. 21–24, Jan. 2016.
- [11] K. Takeuchi, T. Tanaka, and T. Kawabata, "Improvement of BP-based CDMA multiuser detection by spatial coupling," in *Proc. IEEE Int. Symp. Inf. Theory*, St. Petersburg, Russian, Jul 2011, pp. 1489–1493.
- [12] D. Truhachev and C. Schlegel, "Coupling data transmission for multiple-access communications," *IEEE Trans. Inf. Theory*, vol. 65, no. 7, pp. 4550–4574, Jul 2019.
- [13] J. Barbier, C. Schülke, and F. Krzakala, "Approximate message-passing with spatially coupled structured operators, with applications to compressed sensing and sparse superposition codes," *J. Stat. Mech.-Theory Exp.*, vol. 2015, no. 5, p. P05013, May 2015.
- [14] C. Liang, J. Ma, and L. Ping, "Compressed FEC codes with spatial-coupling," *IEEE Commun. Lett.*, vol. 21, no. 5, pp. 987–990, May 2017.
- [15] G. Yue, L. Ping, and X. Wang, "Generalized low-density parity-check codes based on Hadamard constraints," *IEEE Trans. Inf. Theory*, vol. 53, no. 3, pp. 1058–1079, Mar 2007.
- [16] S. Abu-Surra, D. Divsalar, and W. E. Ryan, "Enumerators for protograph-based ensembles of LDPC and generalized LDPC codes," *IEEE Trans. Inf. Theory*, vol. 57, no. 2, pp. 858–886, Feb 2011.
- [17] Li Ping, W. K. Leung, and K. Y. Wu, "Low-rate turbo-Hadamard codes," *IEEE Trans. Inf. Theory*, vol. 49, no. 12, pp. 3213–3224, Dec 2003.
- [18] S. Lin and D. J. Costello, *Error control coding*. Pearson Education India, 2004.
- [19] Q. Huang, S. Chan, L. Ping, and M. Zukerman, "Improving wireless TCP throughput by a novel TCM-Based hybrid ARQ," *IEEE Trans. Wirel. Commun.*, vol. 6, no. 7, pp. 2476–2485, Jul 2007.
- [20] R. Zhang and L. Hanzo, "Superposition-coding-aided multiplexed hybrid ARQ scheme for improved end-to-end transmission efficiency," *IEEE Transactions on Vehicular Technology*, vol. 58, no. 8, pp. 4681–4686, Oct 2009.
- [21] R. Berthier, A. Montanari, and P. M. Nguyen, "State evolution for approximate message passing with non-separable functions," *arXiv:1708.03950*, 2017.
- [22] Y. Ma, C. Rush, and D. Baron, "Analysis of approximate message passing with non-separable denoisers and markov random field priors," *IEEE Trans. Inf. Theory*, vol. 65, no. 11, pp. 7367–7389, Nov 2019.
- [23] A. K. Fletcher, P. Pandit, S. Rangan, S. Sarkar, and P. Schniter, "Plug-in estimation in high-dimensional linear inverse problems: A rigorous analysis," in *Advances in Neural Information Processing Systems*, 2018, pp. 7440–7449.
- [24] K. Bhattad and K. Narayanan, "An MSE-based transfer chart for analyzing iterative decoding schemes using a Gaussian approximation," *IEEE Trans. Inf. Theory*, vol. 53, no. 1, pp. 22–38, Jan. 2007.
- [25] D. Guo, Y. Wu, S. Shamai, and S. Verdú, "Estimation in Gaussian noise: properties of the minimum mean-square error," *IEEE Trans. Inf. Theory*, vol. 57, no. 4, pp. 2371–2385, Apr 2011.
- [26] S. Rangan, "Generalized approximate message passing for estimation with random linear mixing," in *IEEE International Symposium on Information Theory (ISIT)*, Jul 2011, pp. 2168–2172.
- [27] A. Javanmard and A. Montanari, "State evolution for general approximate message passing algorithms, with applications to spatial coupling," *Inf. Inference*, vol. 2, no. 2, pp. 115–144, 2013.

- [28] J. Barbier, M. Dia, and N. Macris, “Universal sparse superposition codes with spatial coupling and GAMP decoding,” *IEEE Trans. Inf. Theory*, vol. 65, no. 9, pp. 5618–5642, Sep. 2019.
- [29] W. K. R. Leung, G. Yue, L. Ping, and X. Wang, “Concatenated zigzag Hadamard codes,” *IEEE Trans. Inf. Theory*, vol. 52, no. 4, pp. 1711–1723, Apr. 2006.
- [30] S. Kudekar, T. J. Richardson, and R. L. Urbanke, “Wave-like solutions of general 1-D spatially coupled systems,” *IEEE Trans. Inf. Theory*, vol. 61, no. 8, pp. 4117–4157, Aug 2015.
- [31] S. Liang, J. Ma, and L. Ping, “Clipping can improve the performance of spatially coupled sparse superposition codes,” *IEEE Commun. Lett.*, vol. 21, no. 12, pp. 2578–2581, Dec 2017.
- [32] E. Biyik, J. Barbier, and M. Dia, “Generalized approximate message-passing decoder for universal sparse superposition codes,” in *IEEE Int. Symp. Inf. Theory (ISIT)*, Jun 2017, pp. 1593–1597.
- [33] J. Barbier, M. Dia, and N. Macris, “Threshold saturation of spatially coupled sparse superposition codes for all memoryless channels,” in *IEEE Inf. Theory Workshop (ITW)*, Sep 2016, pp. 76–80.
- [34] A. Yedla, Y.-Y. Jian, P. S. Nguyen, and H. D. Pfister, “A simple proof of Maxwell saturation for coupled scalar recursions,” *IEEE Trans. Inf. Theory*, vol. 60, no. 11, pp. 6943–6965, Nov 2014.
- [35] C.-K. Wen and K.-K. Wong, “Analysis of compressed sensing with spatially-coupled orthogonal matrices,” *arXiv:1402.3215*, 2014.
- [36] S. Borst, V. Gupta, and A. Walid, “Distributed caching algorithms for content distribution networks,” in *2010 Proceedings IEEE INFOCOM*, March 2010, pp. 1–9.
- [37] L. Ping, L. Liu, K. Wu, and W. K. Leung, “Interleave division multiple-access,” *IEEE Trans. Wirel. Commun.*, vol. 5, no. 4, pp. 938–947, Apr. 2006.
- [38] I. Tal and A. Vardy, “List decoding of polar codes,” *IEEE Trans. Inf. Theory*, vol. 61, no. 5, pp. 2213–2226, May 2015.
- [39] A. Yedla, P. S. Nguyen, H. D. Pfister, and K. R. Narayanan, “Universal codes for the Gaussian MAC via spatial coupling,” in *Proc. Allerton Conf. Commun., Contr. & Comput.*, Monticello, IL, USA, Sep 2011, pp. 1801–1808.
- [40] X. Ma and L. Ping, “Coded modulation using superimposed binary codes,” *IEEE Trans. Inf. Theory*, vol. 50, no. 12, pp. 3331–3343, Dec. 2004.